Journal of Environmental and Engineering Geophysics

June 2020
Volume 25
Issue 2
pp. 000–000
DOI: #10.2113/JEEG19-091

Permafrost Mapping with Electrical Resistivity Tomography: A Case Study in Two Wetland Systems in Interior Alaska

Christopher H. Conaway[1,*], Cordell D. Johnson[2], Thomas D. Lorenson[2], Merritt Turetsky[3], Eugénie Euskirchen[4], Mark P. Waldrop[1] and Peter W. Swarzenski[2,5]

[1]U.S. Geological Survey, 345 Middlefield Road, Menlo Park, CA 94025, USA
[2]U.S. Geological Survey, 400 Natural Bridges Drive, Santa Cruz, CA 95060 USA
[3]Institute of Arctic and Alpine Research, University of Colorado, Campus Box 450, Boulder, CO 80309 USA
[4]Institute of Arctic Biology, University of Alaska Fairbanks, Fairbanks, AK 99775 USA
[5]International Atomic Energy Agency, 4 Quai Antoine 1er, Monaco, 98000, Principality of Monaco

*Corresponding author email: cconaway@usgs.gov

ABSTRACT

Surface-based 2D electrical resistivity tomography (ERT) surveys were used to characterize permafrost distribution at wetland sites on the alluvial plain north of the Tanana River, 20 km southwest of Fairbanks, Alaska, in June and September 2014. The sites were part of an ecologically-sensitive research area characterizing biogeochemical response of this region to warming and permafrost thaw, and the site contained landscape features characteristic of interior Alaska, including thermokarst bog, forested permafrost plateau, and a rich fen. The results show how vegetation reflects shallow (0–10 m depth) permafrost distribution. Additionally, we saw shallow (0–3 m depth) low resistivity areas in forested permafrost plateau potentially indicating the presence of increased unfrozen water content as a precursor to ground instability and thaw. Time-lapse study of June to September suggested a depth of seasonal influence extending several meters below the active layer, potentially as a result of changes in unfrozen water content. A comparison of several electrode geometries (dipole-dipole, extended dipole-dipole, Wenner-Schlumberger) showed that for depths of interest to our study (0–10 m) results were similar, but data acquisition time with dipole-dipole was the shortest, making it our preferred geometry. The results show the utility of ERT surveys to characterize permafrost distribution at these sites, and how vegetation reflects shallow permafrost distribution. These results are valuable information for ecologically sensitive areas where ground-truthing can cause excessive disturbance. ERT data can be used to characterize the exact subsurface geometry of permafrost such that over time an understanding of changing permafrost conditions can be made in great detail. Characterizing the depth of thaw and thermal influence from the surface in these areas also provides important information as an indication of the depth to which carbon storage and microbially-mediated carbon processing may be affected.

INTRODUCTION

Knowledge of the distribution and changing conditions of permafrost in subarctic wetlands is critical to understanding the effects of climate change on the global carbon cycle. This is because there are vast quantities of carbon stored in permafrost: in the northern circumpolar permafrost region, wetland thermokarst landscapes store approximately 164 Pg of soil organic carbon (SOC) in upper 3 m, representing 15% of the total 0–3 m SOC across the region, and the highest average SOC concentration (kg C m–2) relative to other landscape types (Olefeldt *et al.*, 2016). Interior Alaska is in the discontinuous permafrost zone, and changes in permafrost distribution and active layer thickness are already occurring in response to climate change and are projected to continue with future warming (Brown *et al.*, 2015; Douglas *et al.*, 2014). The presence or absence of permafrost is a key control on hydrogeology in this region (Jorgenson *et al.*, 2013; Vonk *et al.*, 2019; Walvoord and Kurylyk, 2016). Permafrost thaw and associated soil moisture changes can drive CO_2 and CH_4 release from soils in boreal ecosystems (Estop-Aragonés *et al.*, 2018; Euskirchen *et al.*, 2017; Natali *et al.*, 2015; 2014; Turetsky *et al.*, 2002), and thaw can release dissolved carbon and nitrogen that affects ecosystem processes (Wickland *et al.*, 2018). Therefore, information on the distribution of ice-rich or thawed subsurface is important in developing an understanding of the biogeochemical response of this region to warming. Here, we describe the use of electrical resistivity tomography (ERT) to examine distribution of permafrost, active layer thickness, and other ecosystem characteristics at two sites on the alluvial plain north of Tanana River (Fig. 1) in June and September of 2014.

Figure 1 View looking southwest across the study area. Photo location is the upper right of location map (Fig. 2). The southern half of the fen area is lower right, and bog site with forested permafrost plateau is center. The open meadow in center left of photo is at the edge of location map. Denali is visible in upper left. Photo credit: Tom Lorenson (USGS).

ERT has proved to be a useful non-intrusive geophysical tool in permafrost studies in the Arctic region, including Alaska (Walvoord and Kurylyk, 2016). For example, a study by Swarzenski *et al.* (2016) concluded that ERT is a useful technique to discern subtle change in surface features over summer thaw cycle on the Arctic coast. Minsley *et al.* (2016) combined multiple geophysical techniques (ERT and NMR) to examine fire effects on near-surface permafrost in boreal landscapes of Interior Alaska, and found the techniques were useful to corroborate remote sensing data. McClymont *et al.* (2013) combined ERT, GPR, and thermal conduction modelling to assess how the land cover distributions influence thawing of discontinuous permafrost. In addition, the application of multiple geophysical methods (ERI, EMI, GPR, infrared) in a permafrost setting was performed by Briggs *et al.* (2017), and the results highlighted the complementary but unique attributes of individual methods. Using a combination ERT, airborne imagery and LiDAR, Douglas *et al.* (2016) demonstrated that ERT can be an effective and rapid means of mapping permafrost.

In this study we investigated permafrost distribution within two experimental wetlands sites near Fairbanks, Alaska that are part of the Bonanza Creek Long Term Ecological Research program. Previous research at these sites has focused on peatland carbon cycling as affected by warming and hydrologic changes (Hultman *et al.*, 2015; McConnell *et al.*, 2013; Neumann *et al.*, 2016; Nicole *et al.*, 2013; Waldrop *et al.*, 2012). Because these sites are ecologically sensitive, a key consideration in our approach was minimizing damage caused through surface or subsurface disturbance, and non-intrusive geophysical methods were considered ideal. Our primary goals were to: i) map shallow permafrost occurrence; ii) identify how vegetation type is related to permafrost within this wetland complex; and iii) examine depth to permafrost and existence of unfrozen areas, or other features useful in understanding or predicting changes in hydrologic connectivity of these wetlands to uplands and the riparian zone related to permafrost degradation.

STUDY SITE

The climate of the Fairbanks area is subarctic, characterized by long, cold winters with a mean air temperature of –22 °C in January, short, mild summers with a mean air temperature of 17 °C in July, and an –2 °C overall mean annual air temperature (ACRC, 2018). The region is in the discontinuous permafrost coverage zone (Jorgenson *et al.*, 2013), and permafrost temperature in the area is relatively warm, near 0 °C (Jorgenson and Osterkamp, 2005). Annual precipitation in 2014 was far above normal (27 cm), with a record summer precipitation of 29 cm (NOAA, 2014), and an annual precipitation of 44 cm for the 3rd wettest year over the 1949–2014 period of record (NOAA, 2015). Precipitation was below normal up until mid-June, when there was a large rainfall event (June 18th–19th) that occurred between our June and September survey and set the record for wettest June for Fairbanks.

The two wetlands sites are on the floodplain north of the Tanana River in the Middle Tanana Valley (Fig. 2) and within the Bonanza Creek Experimental Forest (http://www.lter.uaf.edu/research/study-sites-bcef), about 20 km southeast of Fairbanks, Alaska. One wetland site, hereafter referred to as the "bog" site, included two study profiles (P1 and P2) across thermokarst bog (collapse scar) features and forested permafrost plateau bordered by the transition from the floodplain to hillslope. The second site, the "fen" site, included one profile (P3) that covered a vegetation and soil moisture gradient that transitions across five distinct zones, including a: 1) black spruce forest; 2) low shrub meadow dominated by *Salix* and *Betula* spp.; 3) grass tussock tundra dominated by *Calamagrostis* spp; 4) emergent fen dominated by *Equisetum* and *Carex* species; and 5) moderate rich fen with *Sphagnum*, *Drepanocladus* spp. and *Equisetum* (McConnell *et al.*, 2013; Waldrop *et al.*, 2012).

The study profiles cover several landscape features and geologic deposits (Fig. 3). A surface geologic map for the Tanana Basin (Anderson, 1970) shows the study area is characterized by deposits of aeolian silt

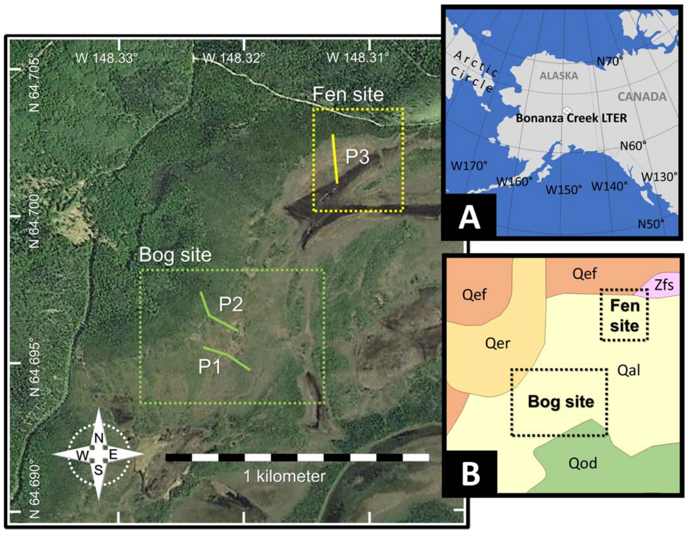

Figure 2 Location of ERT profiles in wetland areas of the Bonanza Creek Experimental Forest, Interior Alaska in June and September 2014 showing bog and fen sites: a) Shows regional location of sites; b) Shows generalized surface geology of the area adapted from Pewe *et al*., (1966) and descriptions by Newberry *et al*., (1996) where *Qer* is re-transported aeolian silt, *Qef* is Fairbanks Loess, *Qal* is floodplain alluvium, *Qod* is organic (wetland) deposits, and *Zfs* is Fairbanks Schist. Imagery from Google Earth Pro, imagery date: 6/1/2017, image credit Landsat / Copernicus.

(Fairbanks Loess); deposits of undifferentiated alluvial, colluvial, or aeolian sand and silt; and igneous and metamorphic rocks mostly represented by the Fairbanks Schist (Newberry *et al*., 1996). Active layer depth along the edge of the alluvial plain north of the Tanana River has been observed at 1.5–6 m, and up to 50 m thick permafrost layers are reported for the edge of the floodplain (Hopkins *et al*., 1955). Beneath peat and organic layers, it is likely that mixed silt, sand, and gravel associated with the floodplain predominate. This alluvium has been characterized by wide heterogeneity in both spatial extent and lithology (Cederstrom, 1963), with no individual deposits more than 5 m thick, and typically much less. Depth to bedrock beneath the alluvial plain in Fairbanks area is greater than 100 m (Cederstrom, 1963). Thermokarst bogs, common in the region, are in localized depressions typically bordered by forest over permafrost (Douglas *et al*., 2016; Jones *et al*., 2013). Fens in the area are often associated with ground water discharge (Racine and Walters, 1994).

METHODS

Data Acquisition

ERT surveys were conducted in both early June (prior to a major rain event) and September 2014 (Table 1). The timing of these surveys was intended to capture the effects of seasonal thaw through one summer. Surface-based 2D resistivity surveys used a SuperSting R8 (AGI, Austin, Texas, USA) and cable with 56 electrodes at 2 m spacing. Profile P1 was collected with two individual ERT surveys (P1a, P1b) overlapping by about 6 m. Short overlaps were used in this study to minimize ground disturbance while maximizing ground coverage. Profile P2 was collected partly along an access boardwalk and was divided into segments (P2a, P2b) with no overlap. A navigation error along the P2a segment in September resulted in a slightly different starting point, about 18 m further west compared to June. The fen site profile P3 was divided into two segments (P3a, P3b) overlapping by about 40 m. Locations for the start and end of each segment were determined using a handheld GPS. Each profile was surveyed using a dipole-dipole (DD) array

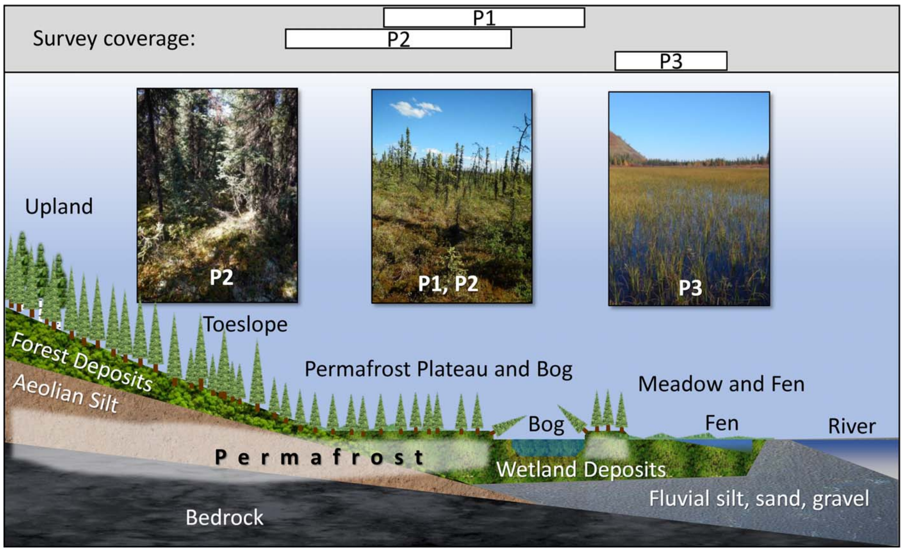

Figure 3 Conceptual profile of landscape and geologic features associated with the profile lines P1, P2, and P3. Photographs from sites are shown. The vertical scale is exaggerated relative to horizontal. See text for details on depth to and thickness of geologic features.

Table 1 List of survey locations and times.

Site	Profile	Segment	Months surveyed	Start latitude	Start longitude	End latitude	End longitude
Bog	P1	a	June	64.69530	−148.32145	64.69476	−148.31952
		b	June	64.69557	−148.32353	64.69527	−148.32135
"	P2	a	June, September	64.69748*	−148.32342*	64.69663	−148.32280
		b	June, September	64.69663	−148.32280	64.69615	−148.32070
Fen	P3	a	June, September	64.70283	−148.31308	64.70175	−148.31283
		b	June	64.70217	−148.31293	64.70118	−148.31272

*starting location for P2a in September was 64.69747 N, −148.32378 W

with a max *n*-spacing of 7. Thaw depth was directly measured along P2 profile in September using a frost probe. These late summer thaw depths are presumed to represent the active layer depth.

Because of the challenge of high resistivity associated with permafrost terrain we employed several electrode array types in September to compare results. During repeat surveys of profile P2 in September, two additional array types were used and compared: extended dipole-dipole (E-DD), and Wenner-Schlumberger (W-S). One benefit of multi-electrode systems is that many array types can easily be selected (Loke *et al.*, 2013). The dipole-dipole (DD) array typically has a relatively fast acquisition time, and better horizontal and depth resolution than a Wenner array, but high ground resistance can limit the effectiveness of the DD array due to weak signal strength (Kneisel, 2006), and Wenner-type arrays are used in some permafrost studies (Briggs *et al.*, 2017; Lewkowicz *et al.*, 2011). The Wenner-Schlumberger (W-S) array can be a compromise between DD and Wenner arrays (Kneisel, 2006). Extended dipole-dipole (E-DD) is a modified DD array selected as an option in the AGI command file with about twice the amount of apparent resistivity data points.

A contact resistance test was preformed prior to each survey. Contact resistance values at the bog site in June were sometimes high (5,000–10,000 ohms), typically where spikes were driven into ice or icy material. This high resistance was expected to decrease overall data quality due to lower electric current injected into the ground, in turn producing a lower signal-to-noise ratio. September values at the bog site were usually <5000 ohms, and values for the fen site were <2,500 ohms for both June and September surveys.

Data Analysis Methods

Data analysis was performed with AGI EarthImager 2D Version 2.4.4 (Build 649). Transitions from permafrost to thaw were expected to create sharp spatial contrasts in resistivity (Lewkowicz *et al.*, 2011; Loke *et al.*, 2003), and high-resistivity permafrost was expected to give a lower signal-to-noise ratio relative to unfrozen ground , so robust inversion method was used because it performs better with such boundaries and noisy data (AGI, 2009). Typically, 6–8 iterations were performed with a resulting RMS in the range of 5–10%, which is typical in a permafrost environment (Minsley *et al.*, 2016; Swarzenski *et al.*, 2016). Time lapse inversions were carried out using difference inversion (AGI, 2009), which combines the inversion of the base dataset (June) and the monitor dataset (September) in one step. The results of the time lapse inversions are given as percent difference in resistivity. The models in this study were not adjusted for changes in ground surface elevation, however there is little change in elevation (< 3 m) across the segments at the sites and little microtopograpy (Chivers *et al.*, 2009).

To assess the reliability of the results, we examined the relative model sensitivity for our inversions and considered data assessment results from other studies in similar settings. The relative model sensitivity gives semi-quantitative assessment of data reliability, with higher values indicating more reliable results. Relative model sensitivity sections generated using EarthImager 2D are overlaid on the associated inverted resistivity sections. Results from studies in similar lowland permafrost settings using surface-based ERT and 1–2 m electrode suggest that data may typically be useful to a depth of 5–10 m (Briggs *et al.*, 2017; Minsley *et al.*, 2016; Oldenborger and LeBlanc, 2018).

Landform and Vegetation Zones

The approximate boundaries of vegetation zones or thermokarst bog versus permafrost plateau were interpreted by a combination of field observations along the ERT profiles, visual inspection of satellite imagery using Google Earth Pro (version 7.3.0.3832), and data from other reports (2017; Manies *et al.*, 2016). The approximate location of the break between hillslope and floodplain at the bog site was determined using data from hand-held GPS, a USGS topographic map (FAIRBANKS C-3 NW, AK 2013 Quadrangle), and terrain viewed using Google Earth Pro.

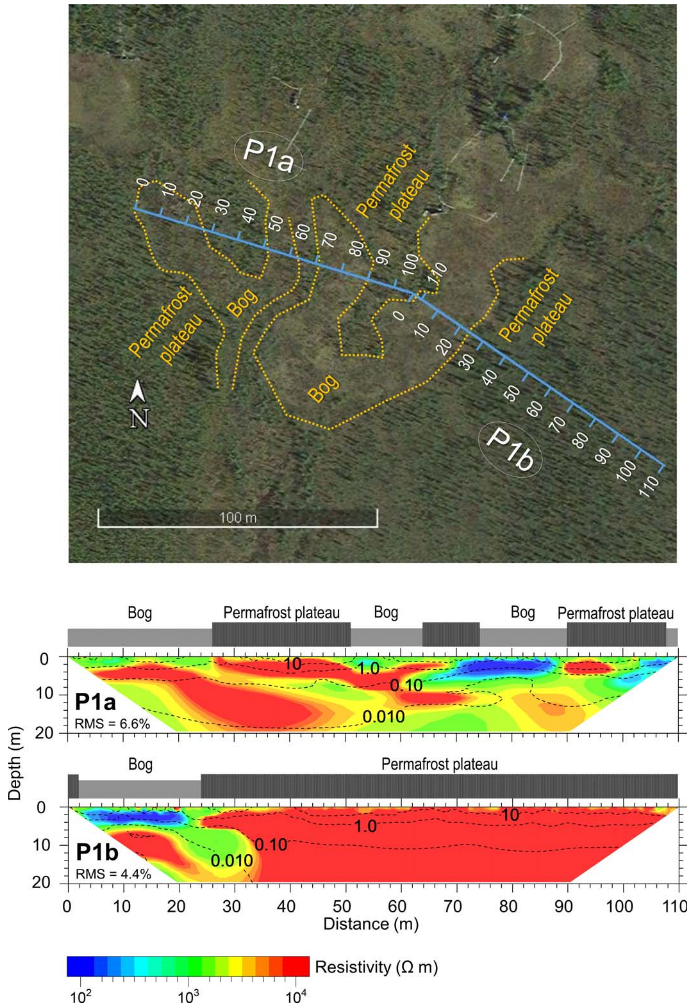

Figure 4 Upper: profile across the southern part of the bog site, divided into P1a and P1b segments, shown by blue hatched lines. Hatch marks and values denote distance in meters. Dotted lines show approximate boundaries between thermokarst bog and permafrost plateau. Map Imagery from Google Earth Pro, imagery date: 6/1/2017, image credit Landsat / Copernicus. Lower: vegetation types and inverted resistivity sections with model root mean square (RMS) error for P1a and P1b in June 2014. Colors on sections indicate resistivity, and dashed contour lines show order of magnitude changes in relative model sensitivity.

Resistivity as an Indicator of Frozen Material

Unfrozen resistivity of water-saturated peat and other unconsolidated material is mainly dependent on the saturating fluid resistivity, and to a lesser extent on water saturation (Ponziani *et al.*, 2012). Resistivity in such material increases exponentially at the freezing point of water until the pore water is frozen (1975; Hoekstra *et al.*, 1974), however some pore water can remain unfrozen at subfreezing conditions even at relatively low temperatures (Hauck, 2002; Oldenborger and LeBlanc, 2018). Resistivity of frozen, saturated material is also dependent on ice volume and temperature (Hoekstra *et al.*, 1975). At the end of the growing season (September) in this region, active layer soils are typically unfrozen and permafrost temperature is near 0 °C (Jorgenson and Osterkamp, 2005). Thus, the high resistivity values (>1000 ohm-m) observed in this study represent frozen, ice-rich material. It is important to note, however, that the changes in resistivity from >1000 ohm-m down to 200 ohm-m are not necessarily an indicator of thaw, as resistivity of saturated frozen material can decrease nearly an order of magnitude from –2 to 0 °C in peat and silt with varying organic content that are characteristic in the subsurface of the study area (Hoekstra *et al.*, 1974). This range reflects the presence of unfrozen water, and modeling studies and observations of subsurface in Bonanza Creek area show that unfrozen water can exist both in the frozen active layer and near-surface permafrost (Minsley *et al.*, 2016; Romanovsky and Osterkamp, 2000). This unfrozen water can decrease resistivity and may be an indicator of permafrost vulnerability and evolution (Oldenborger and LeBlanc, 2018). Material with resistivity <200 ohm-m is very likely thawed in this setting.

RESULTS AND DISCUSSION

Permafrost Distribution and Vegetation

Differences in vegetation or landscape type reflect the presence or absence of shallow permafrost in this study. This relationship is definitively shown over hundreds of meters in the bog area by ERT data. The P1 profile across the bog site (Fig. 4) represents alternating thermokarst (collapse scar) bog and forested permafrost plateau (intact surface permafrost). The P1a segment runs across several transitions between thermokarst bog and permafrost plateau, and the P1b segment runs from thermokarst area into an area predominantly of sparse, stunted black spruce permafrost plateau. The bog areas along this profile are underlain by less resistive (<1000 ohm-m) material, at times with large thaw features with resistivity <200 ohm-m down to 5 m depth. In contrast to this low-resistivity area, the area of stunted black spruce is characterized by highly-resistive ice-rich material very nearly to the surface that was observed when installing metal spikes for the resistivity electrodes.

The changes with landscape type and resistivity are also observed moving from the edge of the hillslope (toeslope) onto the floodplain. Moving from northwest to southeast on the P2 profile of the bog site (Fig. 5), the P2a segment begins in spruce forest on the toeslope (*Picea mariana and P. glauca*) and ground elevation lowers slightly as it transitions into floodplain permafrost plateau. The P2b segment begins in that permafrost plateau and continues into

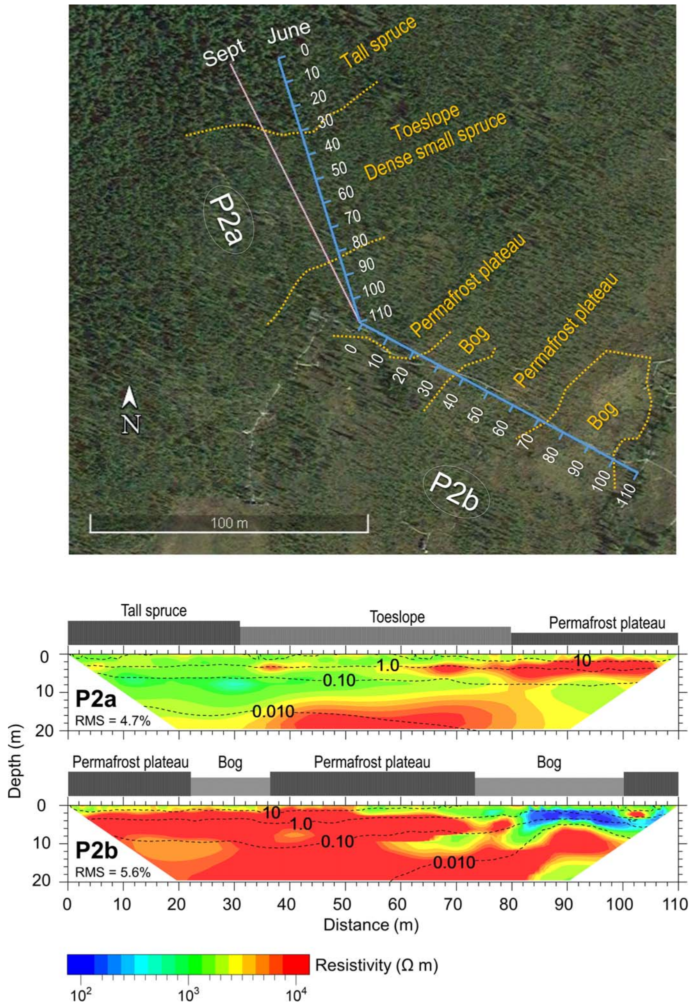

Figure 5 Upper: Profile across the northern part of the bog site, divided into P2a and P2b segments, shown by blue hatched lines showing distance in meters. P2a in September had a slightly different trend than in June. Dotted lines show boundaries between hillslope, thermokarst bog, and permafrost plateau. Imagery from Google Earth Pro, imagery date: 6/1/2017, Landsat / Copernicus. Lower: vegetation types and inverted resistivity sections with model root mean square (RMS) error for P2a and P2b in June 2014. Colors on sections indicate resistivity, and dashed contour lines show order of magnitude changes in relative model sensitivity.

an area of alternating thermokarst bog and forested permafrost plateau.

As with P1, the open bog areas along P2b are thermokarst bog, with large thaw features with less resistive (*i.e.*, unfrozen) material to a depth of 5–10 m that represent collapse scar features and the replacement of permafrost plateau by open bog (Jones *et al.*, 2013), and the forested permafrost plateau with stunted black spruce is underlain by more resistive material likely representing permafrost (Fig. 5). Since 2014, the area on P2b from about 50–72 m has had spruce dieback and collapsed into bog. This area was slightly less resistive (<3,000 ohm-m) from 0–3 m depth compared to much of the 0–50 m distance along the P2b segment, potentially indicating a precursor to ground instability and thaw. Thus, the ERT survey is potentially useful in showing permafrost vulnerable to collapse or in the process of collapsing, but multi-annual time-series ERT data in degrading permafrost plateau environment are needed to fully explore this idea.

Differences in subsurface resistivity across the vegetation gradient profile at the fen site are subtler than those at the bog site. The P3 segment begins in black spruce permafrost forest with feather moss and lichen ground cover, and then transitions into low shrub consisting of stunted birch, willow, and aspen. From there grass tussocks are the predominant feature until again there is a transition to emergent fen, and then finally a rich fen with predominantly sedge (Fig. 6). This vegetation gradient reflects a gradient of soil moisture conditions related to water table position and drainage (Manies *et al.*, 2016; McConnell *et al.*, 2013; Waldrop *et al.*, 2012). The near surface (0–5 m) in the forest is less resistive than the sparse shrub area, and this difference likely represents shallower depth to seasonal ice-saturated material in the low shrub area, ice content changes, or soil composition changes. The near surface in the emergent fen is somewhat less resistive than the rest of the P3a profile, likely representing being submerged much of the year, and the rich fen shows large thaw feature.

The relationship between shallow permafrost and vegetation type was also demonstrated in the nearby Tanana Flats Lowland by Douglas *et al.* (2016). Thus, vegetation is strong indicator of shallow permafrost across the Tanana Valley floodplain. In addition, the results show that thaw depths in the thermokarst in this area are typically about 5 m. Vegetation is less useful for assessing the distribution of this deeper permafrost (Douglas *et al.*, 2016). This information is valuable, because the upper 1–2 m of the wetland sites in this study are fairly well characterized by coring (2017; Manies *et al.*, 2016), but little information is available for greater depths. This information is also valuable because it is an indication of the depth to which carbon storage may be affected, potentially through the mobilization of dissolved organic carbon from thawing material (Drake *et al.*, 2015; Wickland *et al.*, 2018). Overall, permafrost appeared to be present at some depth beneath all the bog area sites, and along the P3a segment of the profile at the fen site. This is consistent with previous observations noting the depth to permafrost as 1.5–6 m along the edge of the alluvial plain north of the Tanana River (Hopkins *et al.*, 1955).

Late Summer Survey Results (September) and Seasonal Changes

An analysis using time lapse inversion of the June versus September surveys along the P2a, P2b, and P3a segment (Fig. 7) shows there is a general change to

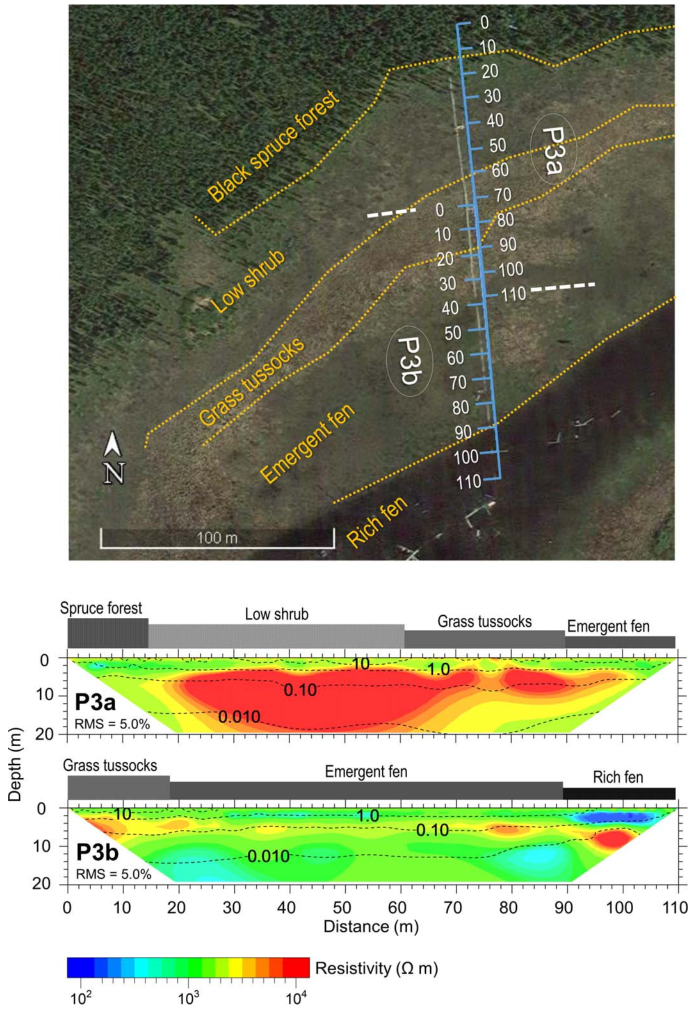

Figure 6 Upper: vegetation gradient profile across the fen site, divided into P3a and P3b segments, shown by blue hatched lines. Segments overlap by 36 m. Hatch marks and values denote distance in meters. Dotted lines show boundaries between vegetation gradient areas. Imagery from Google Earth Pro, imagery date: 6/1/2017, image Landsat / Copernicus. Lower: vegetation types and inverted resistivity sections with model root mean square (RMS) error for P3a and P3b in June 2014. Colors on sections indicate resistivity, and dashed contour lines show order of magnitude changes in relative model sensitivity.

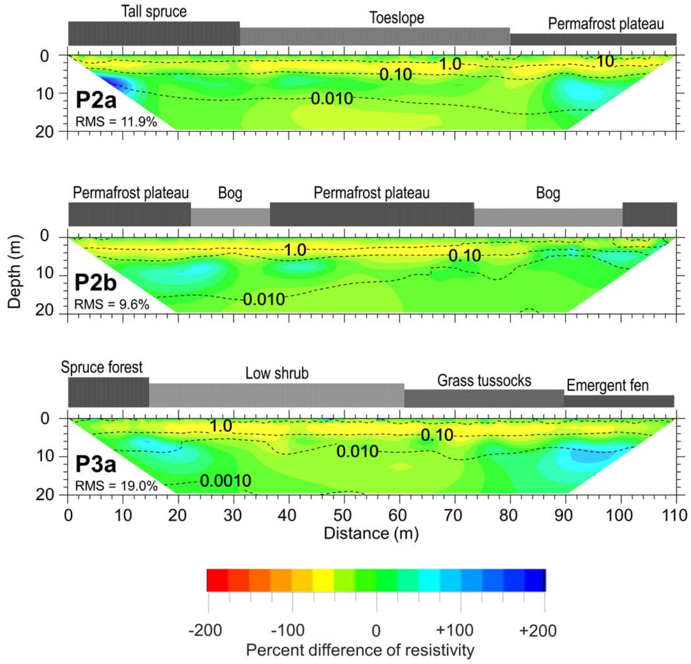

Figure 7 Time lapse inversion models with model root mean square (RMS) error for June to September along the P2a, P2b, and P3a segments. Colors on sections indicate percent difference in resistivity and dashed contour lines show order of magnitude changes in relative model sensitivity. Vegetation types for each segment are shown for reference.

lower modeled resistivity values (resulting in a negative value for percent difference of resistivity) from the surface to a depth of about 5 m along most of the segments. The P3b segment area was flooded in September, and a repeat survey was not performed there. This change in part reflects the thawing of the active layer, although as discussed later this thaw is typically limited to the upper 1 m. The persistence of observed changes beyond 1 m depth may be the result of changes in unfrozen water content beneath the active layer, and potentially changes in water saturation because of record summer precipitation levels, or potentially measurement or inversion artifacts due to the highly resistive environment. Although changes in resistivity and frozen water content occurring several meters below the active layer have been observed in other settings where permafrost is near 0 °C (Hauck, 2002; Hilbich *et al.*, 2011; Oldenborger and LeBlanc, 2018), for our study we must acknowledge the possibility that the observed change may be mostly, or in part, a result of measurement difficulties, *e.g.*, the high contact resistance encountered in June P2 surveys. Observed increases in resistivity at $>$ 6 m depth are associated with relatively low model sensitivity, and thus less reliable data and are presumably modeling artifacts.

Array Comparisons

The inversion models from the various array produced minor differences. These differences included the thickness of some near-surface (0–5 m) low-resistivity areas, and the presence or absence of features. For example, in the P2a array comparisons (Fig. 8) from 0–40 m distance a modeled resistivity of $\leq$500 ohm-m occurs to a depth of 10 m with DD, but only to 2 m with W-S. A similar example is in the P2b array comparison (Fig. 9) beneath the bog area from 80–100 m distance. Another example is a relatively low resistivity spot in P2b at 40 m distance and 8 m depth that is present in DD and E-DD but absent in the W-S results.

Many of the minor differences observed between DD, E-DD, and W-S surveys are likely related to data

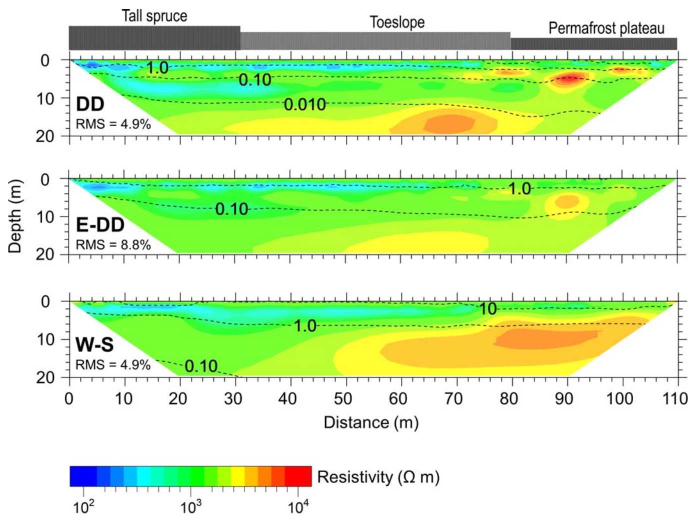

Figure 8 Inverted resistivity sections with model root mean square (RMS) error for the P2a segment in September using three array types: dipole-dipole (DD), extended dipole-dipole (E-DD), and Wenner-Schlumberger (W-S). Colors on sections indicate resistivity, and dashed contour lines show order of magnitude changes in relative model sensitivity. Vegetation types for the segment are shown for reference.

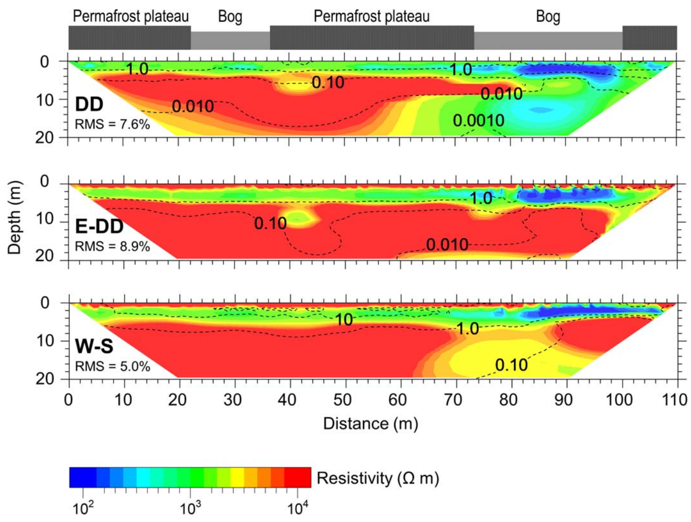

Figure 9 Inverted resistivity sections with model root mean square (RMS) error for the P2b segment in September using three array types: dipole-dipole (DD), extended dipole-dipole (E-DD), and Wenner-Schlumberger (W-S). Colors on sections indicate resistivity, and dashed contour lines show order of magnitude changes in relative model sensitivity. Vegetation types for the segment are shown for reference.

collection and processing, and reflect overall data quality, inversion settings, and model sensitivity with depth. For example, there were fewer data layers from 0–3 m depth (*i.e.*, across the active layer) in from the W-S survey compared to DD or E-DD, but signal strength was typically much higher with W-S. Resolution of the above-mentioned differences based on array type remain to be matched with other geophysical data or ground-truthing and investigated with forward modelling techniques. Major features in near surface, such as those associated with forested permafrost plateau versus bog and the deep thaw at the bog site P2b segment from 80–100 m, are similar across all the DD, E-DD, and W-S results. Despite the potential issue of highly-resistive permafrost limiting effectiveness of DD array (Kneisel, 2006), for studying relatively shallow features associated with landscape evolution at this site there appears to be no clear advantage in the results using the E-DD or W-S array. Consequently, the relatively fast acquisition time of DD array gives it preference.

Active Layer Depth

Although the ERT data collected here are useful in identifying general permafrost distribution, especially as far as areal extension, our methods were not ideal for precisely defining active layer depth. Thaw depth measurements were made using a frost probe across the bog site throughout June to September 2014, but measurements in direct association with the ERT profiles were limited to profile P2 in September. Late summer (September) thaw depth measurements are considered to best capture active layer depth. In June 2014 probe depths within the forest hillslope area were approximately 25 cm and increased to 50 cm in mid-August. In September, along the first 10 m of the P2a segment probe depths were 80–130 cm, then 60 ± 7 cm for measurements along the rest of the segment. In the bog area, the probe depths in June also averaged 25 cm, thawed out to >200 cm by the beginning of July, such that the depth to mineral soil in the September trip was approximately 150 cm. Frost probe depths taken along the P2b segment in September were 59 ± 8 cm for 0–50 m along the segment, increasing in depth to about 70 cm for 60–80 m, and >200 cm from 100–110 m. Frost probe thaw depth measurements at the fen site were not measured in 2014, but in previous years active layer depth measurements showed that only the black spruce forest and low shrub contained permafrost with active layer depths generally less than 50 cm (Waldrop *et al.*, 2012). Observed summer thaw depths up to 1 m are reported for the rich fen area (Kane *et al.*, 2010) and elsewhere in the alluvial plain of the Tanana River (Hopkins *et al.*, 1955).

The depth to frozen material, and by extension the depth of the active layer, is not generally expected to be well-resolved with ERT because this depth is not uncommonly ≤100 cm and there were few very near-surface ERT data layers in our surveys. For example, the shallowest three data layers for the DD and E-DD surveys were at $z = 1.0$ m, 1.5 m, 2.0 m, and the shallowest two layers for W-S are at $z = 1.3$ m and 2.5 m. Thaw depth estimates using ERT data can be made by using typical minimum estimates of 600–1000 ohm-m for permafrost resistivity in the Fairbanks area (Douglas *et al.*, 2016). However, data on resistivity on saturated soils of the Fairbanks area show that both Fairbanks Loess and silt with substantial mineral content can have a lower resistivity (200–600 ohm-m) than peat (600 ohm-m) at temperatures very near 0 °C (Hoekstra *et al.*, 1974). At the bog site, a peat to mineral soil transition occurs in in the top 1–2 m (Manies *et al.*, 2017). In addition to data resolution issues described above, the difficulty in precisely resolving active layer depth using ERT would also involve a detailed understanding of the soil profile characteristics. Thus, investigation and resolution the active layer is likely better achieved using a frost probe in our study area and other areas with thaw depths < 1 m. Briggs *et al.* (2017) compared electrical resistivity data collected in a permafrost landscape using both 2.0 m and 0.5 m electrode spacing and found that data from the latter spacing greatly improved the matching with frost probe data from < 2 m, however the depth of investigation using that closer electrode spacing was limited to 3 m.

Small-scale Subsurface Variability and Hydrologic Connections

The resistivity data did not appear to conclusively highlight any lithological differences, such as sand or gravel layers. Such layers might serve as hydrologic connections as permafrost thaws and talik forms. A previous investigation of saturated organic soils of the Fairbanks area suggests that the range of resistivity as a function of temperature observed in some peat samples spans that observed in saturated sand and gravel over similar temperatures (Hoekstra *et al.*, 1974). Saturated sand and gravel can have higher resistivity across a range of temperatures than Fairbanks Loess, but could perhaps be comparable when there is substantial organic matter content in the silt (Hoekstra *et al.*, 1974). Although sand and gravel layers are expected to occur in this study area based on generalized cross sections (Douglas *et al.*, 2014) and information from elsewhere on the floodplain (Cederstrom, 1963), the contrast in resistivity may be too small to resolve, or their occurrence at depth may be masked by high-resistivity of the near-surface.

CONCLUSION

Overall, the results highlight the utility of ERT surveys to rapidly characterize permafrost distribution and thaw features in permafrost peatlands in Interior Alaska. The data show that shallow (0–10 m) permafrost distribution is reflected in vegetation composition, but important characteristics are also detected: that of permafrost being thawed from below, permafrost nearing collapse, and surface features creating new water tracks or wetlands. Showing the relationship between shallow permafrost and vegetation is important in this area because it is ecologically sensitive, and ground-truthing can cause excessive disturbance, whereas vegetation can be mapped from aerial surveys or remote sensing (Douglas *et al.*, 2016). We believe our observation of shallow (0–3 m depth) low resistivity permafrost in forested permafrost plateau were potentially indicating the presence of greater unfrozen water content and thus can be used as an indicator to ground instability and thaw. Time-lapse study of June to September suggested a depth of seasonal influence extending several meters below the active layer, potentially as a result of changes in unfrozen water content. Characterizing the depth of thaw and thermal influence from the surface in thermokarst areas provides important information as it is an indication of the depth to which carbon storage and microbially-mediated carbon processing may be affected. A comparison of several electrode geometries (dipole-dipole, extended dipole-dipole, Wenner-Schlumberger) suggested that for depths of interest to our study (0–10 m) results were similar, but data acquisition time with dipole-dipole was the shortest, making it our preferred method for the site. Resolution of the active layer (typically ≤100 cm) was better achieved using a frost probe in our study area compared to the use of ERT. But ERT allows for a detailed understanding of the distribution and vulnerability of permafrost deeper in the soil profile. Multi-year observations along the same transects will allow us to discern whether hypotheses of vulnerable permafrost made from ERT data are supported or not. Studies by others combining state-of-the-art geophysical techniques and soil monitoring are currently underway at the Bonanza Creek site (James *et al.*, 2019a; 2019b)

References

ACRC, 2018, Fairbanks Annual Weather Review 2014 by The Alaska Climate Research Center: http://akclimate.org/Summary/Annual/Fairbanks/2014 Date accessed May 11, 2018

AGI, 2009, Instruction Manual for EarthImager 2D Version 2.4.0: Advanced Geosciences, Inc., Austin, Texas.

Anderson, G.S., 1970, Hydrologic reconnaissance of the Tanana basin, central Alaska: 319, U.S. Geological Survey, Washington, D.C.

Briggs, M.A., Campbell, S., Nolan, J., Walvoord, M.A., Ntarlagiannis, D., Day-Lewis, F.D., and Lane, J.W., 2017, Surface geophysical methods for characterising frozen ground in transitional permafrost landscapes: Permafrost and Periglacial Processes, **28**, 52–65.

Brown, D.R.N., Jorgenson, M.T., Douglas, T.A., Romanovsky, V.E., Kielland, K., Hiemstra, C., Euskirchen, E.S., and Ruess, R.W., 2015, Interactive effects of wildfire and climate on permafrost degradation in Alaskan lowland forests: Journal of Geophysical Research-Biogeosciences, **120**, 1619–1637.

Cederstrom, D.J., 1963, Ground-water resources of the Fairbanks area, Alaska: 1590, U.S. Geological Survey, Washington, D.C., 84 pp.

Chivers, M.R., Turetsky, M.R., Waddington, J.M., Harden, J.W., and McGuire, A.D., 2009, Effects of experimental water table and temperature manipulations on ecosystem CO_2 fluxes in an Alaskan rich fen: Ecosystems, **12**, 1329–1342.

Douglas, T.A., Jones, M.C., and Hiemstra, C.A., 2014, Sources and sinks of carbon in boreal ecosystems of interior Alaska: a review: Elementa: Science of the anthropocene, **2**.

Douglas, T.A., Jorgenson, M.T., Brown, D.R.N., Campbell, S.W., Hiemstra, C.A., Saari, S.P., Bjella, K., and Liljedahl, A.K., 2016, Degrading permafrost mapped with electrical resistivity tomography, airborne imagery and LiDAR, and seasonal thaw measurements: Geophysics, **81**, Wa71–Wa85.

Drake, T.W., Wickland, K.P., Spencer, R.G.M., McKnight, D.M., and Striegl, R.G., 2015, Ancient low-molecular-weight organic acids in permafrost fuel rapid carbon dioxide production upon thaw: Proceedings of the National Academy of Sciences of the United States of America, **112**, 13946–13951.

Estop-Aragonés, C., Cooper, M.D.A., Fisher, J.P., Thierry, A., Garnett, M.H., Charman, D.J., Murton, J.B., Phoenix, G.K., Treharne, R., Sanderson, N.K., Burn, C.R., Kokelj, S.V., Wolfe, S.A., Lewkowicz, A.G., Williams, M., and Hartley, I.P., 2018, Limited release of previously-frozen C and increased new peat formation after thaw in permafrost peatlands: Soil Biology & Biochemistry, **118**, 115–129.

Euskirchen, E.S., Bret-Harte, M.S., Shaver, G.R., Edgar, C.W., and Romanovsky, V.E., 2017, Long-term release of carbon dioxide from arctic tundra ecosystems in Alaska: Ecosystems, **20**, 960–974.

Hauck, C., 2002, Frozen ground monitoring using DC resistivity tomography: Geophysical Research Letters, **29**, 12–1–12-4.

Hilbich, C., Fuss, C., and Hauck, C., 2011, Automated time-lapse ERT for improved process analysis and monitoring of frozen ground: Permafrost and Periglacial Processes, **22**, 306–319.

Hoekstra, P., Sellmann, P.V., and Delaney, A., 1975, Ground and airborne resistivity surveys of permafrost near Fairbanks, Alaska: Geophysics, **40**, 641–656.

Hoekstra, P., Sellmann, P.V., and Delaney, A.J., 1974, Airborne Resistivity Mapping of Permafrost Near Fairbanks, Alaska: Research Report 324, U.S. Army Cold Regions Research and Engineering Laboratory, Hanover, New Hampshire, 51 pp.

Hopkins, D.M., Karlstrom, T.N.V., Black, R.F., Williams, J.R., Péwé, T.L., Fernald, A.T., and Muller, E.H., 1955, Permafrost and ground water in Alaska: U.S. Geological Survey Professional Paper 264-F, 146 pp.

Hultman, J., Waldrop, M.P., Mackelprang, R., David, M.M., McFarland, J., Blazewicz, S.J., Harden, J., Turetsky, M.R., McGuire, A.D., Shah, M.B., VerBerkmoes, N.C., Lee, L.H., Mavrommatis, K., and Jansson, J.K., 2015, Multi-omics of permafrost, active layer and thermokarst bog soil microbiomes: Nature, **521**, 208.

James, S.R., Knox, H.A., Abbott, R.E., Panning, M.P., and Screaton, E.J., 2019a, Insights Into Permafrost and Seasonal Active-Layer Dynamics From Ambient Seismic Noise Monitoring: Journal of Geophysical Research: Earth Surface, **124**, 1798–1816.

James, S.R., Minsley, B.J., Waldrop, M.P., and Mcfarland, J.W., 2019b, Understanding the importance of water and ice dynamics at a thermokarst site with novel geophysical observations: American Geophysical Union 2019 Fall Meeting, San Francisco, CA, USA.

Jones, M.C., Booth, R.K., Yu, Z., and Ferry, P., 2013, A 2200-year record of permafrost dynamics and carbon cycling in a collapse-scar bog, Interior Alaska: Ecosystems, **16**, 1–19.

Jorgenson, M.T., Harden, J., Kanevskiy, M., O'Donnell, J., Wickland, K., Ewing, S., Manies, K., Zhuang, Q.L., Shur, Y., Striegl, R., and Koch, J., 2013, Reorganization of vegetation, hydrology and soil carbon after permafrost degradation across heterogeneous boreal landscapes: Environmental Research Letters, **8**.

Jorgenson, M.T., and Osterkamp, T.E., 2005, Response of boreal ecosystems to varying modes of permafrost degradation: Canadian Journal of Forest Research-Revue Canadienne De Recherche Forestiere, **35**, 2100–2111.

Kane, E.S., Turetsky, M.R., Harden, J.W., McGuire, A.D., and Waddington, J.M., 2010, Seasonal ice and hydrologic controls on dissolved organic carbon and nitrogen concentrations in a boreal-rich fen: Journal of Geophysical Research-Biogeosciences, **115**.

Kneisel, C., 2006, Assessment of subsurface lithology in mountain environments using 2D resistivity imaging: Geomorphology, **80**, 32–44.

Lewkowicz, A.G., Etzelmuller, B., and Smith, S.L., 2011, Characteristics of discontinuous permafrost based on ground temperature measurements and electrical resistivity tomography, Southern Yukon, Canada: Permafrost and Periglacial Processes, **22**, 320–342.

Loke, M.H., Acworth, I., and Dahlin, T., 2003, A comparison of smooth and blocky inversion methods in 2D electrical imaging surveys: Exploration Geophysics, **34**, 182–187.

Loke, M.H., Chambers, J.E., Rucker, D.F., Kuras, O., and Wilkinson, P.B., 2013, Recent developments in the direct-current geoelectrical imaging method: Journal of Applied Geophysics, **95**, 135–156.

Manies, K.L., Fuller, C.C., Jones, M.C., Waldrop, M.P., and McGeehin, J.P., 2017, Soil data for a thermokarst bog and the surrounding permafrost plateau forest, located at Bonanza Creek Long Term Ecological Research Site, Interior Alaska: 2016-1173, Reston, VA, 1–11 pp.

Manies, K.L., Harden, J.W., Fuller, C.C., Xu, X., and McGeehin, J.P., 2016, Soil data for a vegetation gradient located at Bonanza Creek Long Term Ecological Research Site, interior Alaska: 2016-1034, Reston, VA, 16 pp.

McClymont, A.F., Hayashi, M., Bentley, L.R., and Christensen, B.S., 2013, Geophysical imaging and thermal modeling of subsurface morphology and thaw evolution of discontinuous permafrost: Journal of Geophysical Research: Earth Surface, **118**, 1826–1837.

McConnell, N.A., Turetsky, M.R., McGuire, A.D., Kane, E.S., Waldrop, M.P., and Harden, J.W., 2013, Controls on ecosystem and root respiration across a permafrost and wetland gradient in interior Alaska: Environmental Research Letters, **8**.

Minsley, B.J., Pastick, N.J., Wylie, B.K., Brown, D.R.N., and Kass, M.A., 2016, Evidence for nonuniform permafrost degradation after fire in boreal landscapes: Journal of Geophysical Research: Earth Surface, **121**, 2015JF003781.

Natali, S.M., Schuur, E.A.G., Mauritz, M., Schade, J.D., Celis, G., Crummer, K.G., Johnston, C., Krapek, J., Pegoraro, E., Salmon, V.G., and Webb, E.E., 2015, Permafrost thaw and soil moisture driving CO_2 and CH_4 release from upland tundra: Journal of Geophysical Research: Biogeosciences, **120**, 525–537.

Neumann, R.B., Blazewicz, S.J., Conaway, C.H., Turetsky, M.R., and Waldrop, M.P., 2016, Modeling CH_4 and CO_2 cycling using porewater stable isotopes in a thermokarst bog in Interior Alaska: Results from three conceptual reaction networks: Biogeochemistry, **127**, 57–87.

Newberry, R.J., Bundtzen, T.K., Clautice, K.H., Combellick, R.A., Douglas, T., Laird, G.M., Liss, S.A., Pinney, D.S., Reifenstuhl, R.R., and Solie, D.N., 1996, Preliminary geologic map of the Fairbanks mining district, Alaska: Alaska Division of Geological & Geophysical Surveys Public Data File 96–16.

Nicole, A.M., Merritt, R.T., McGuire, A.D., Evan, S.K., Mark, P.W., and Jennifer, W.H., 2013, Controls on ecosystem and root respiration across a permafrost and wetland gradient in interior Alaska: Environmental Research Letters, **8**, 045029.

NOAA, 2014, NOAA National Centers for Environmental Information, State of the Climate: National Climate Report for August 2014, published online September 2014, retrieved on November 7, 2018 from https://www.ncdc.noaa.gov/sotc/national/201408.

NOAA, 2015, NOAA National Centers for Environmental Information, State of the Climate: National Climate Report for Annual 2014, published online January 2015, retrieved on November 7, 2018 from https://www.ncdc.noaa.gov/sotc/national/201413.

Oldenborger, G.A., and LeBlanc, A.-M., 2018, Monitoring changes in unfrozen water content with electrical resistivity surveys in cold continuous permafrost: Geophysical Journal International, **215**, 965–977.

Olefeldt, D., Goswami, S., Grosse, G., Hayes, D., Hugelius, G., Kuhry, P., McGuire, A.D., Romanovsky, V.E., Sannel, A.B.K., Schuur, E.A.G., and Turetsky, M.R., 2016, Circumpolar distribution and carbon storage of thermokarst landscapes: Nature Communications, **7**, 13043.

Péwé, T.L., Wahraftig, C., and Weber, F.R., 1966, Geologic map of the Fairbanks quadrangle, Alaska, Miscellaneous Geologic Investigations Map I-455. U.S. Geological Survey.

Ponziani, M., Slob, E.C., and Ngan-Tillard, D.J.M., 2012, Experimental validation of a model relating water content to the electrical conductivity of peat: Engineering Geology, **129–130**, 48–55.

Racine, C.H., and Walters, J.C., 1994, Groundwater-discharge fens in the Tanana Lowlands, Interior Alaska USA: Arctic and Alpine Research, **26**, 418–426.

Romanovsky, V.E., and Osterkamp, T.E., 2000, Effects of unfrozen water on heat and mass transport processes in the active layer and permafrost: Permafrost and Periglacial Processes, **11**, 219–239.

Swarzenski, P.W., Johnson, C.D., Lorenson, T.D., Conaway, C.H., Gibbs, A.E., Erikson, L.H., Richmond, B.M., and Waldrop, M.P., 2016, Seasonal electrical resistivity surveys of a coastal bluff, Barter Island, North Slope Alaska: Journal of Environmental & Engineering Geophysics, **21**, 37–42.

Turetsky, M.R., Kotowska, A., Bubier, J., Dise, N.B., Crill, P., Hornibrook, E.R.C., Minkkinen, K., Moore, T.R., Myers-Smith, I.H., Nykanen, H., Olefeldt, D., Rinne, J., Saarnio, S., Shurpali, N., Tuittila, E.S., Waddington, J.M., White, J.R., Wickland, K.P., and Wilmking, M., 2014, A synthesis of methane emissions from 71 northern, temperate, and subtropical wetlands: Global Change Biology, **20**, 2183–2197.

Turetsky, M.R., Wieder, R.K., and Vitt, D.H., 2002, Boreal peatland C fluxes under varying permafrost regimes: Soil Biology & Biochemistry, **34**, 907–912.

Vonk, J.E., Tank, S.E., and Walvoord, M.A., 2019, Integrating hydrology and biogeochemistry across frozen landscapes: Nature Communications, **10**: 5377.

Waldrop, M.P., Harden, J.W., Turetsky, M.R., Petersen, D.G., McGuire, A.D., Briones, M.J.I., Churchill, A.C., Doctor, D.H., and Pruett, L.E., 2012, Bacterial and enchytraeid abundance accelerate soil carbon turnover along a lowland vegetation gradient in interior Alaska: Soil Biology & Biochemistry, **50**, 188–198.

Walvoord, M.A., and Kurylyk, B.L., 2016, Hydrologic impacts of thawing permafrost—a review: Vadose Zone Journal, **15**.

Wickland, K.P., Waldrop, M.P., Aiken, G.R., Koch, J.C., Jorgenson, M., and Striegl, R.G., 2018, Dissolved organic carbon and nitrogen release from boreal Holocene permafrost and seasonally frozen soils of Alaska: Environmental Research Letters, **13**.

Acknowledgments

The authors gratefully acknowledge the current and past efforts of other senior investigators on the APEX project, and other collaborators, including David McGuire, Jennifer Harden, Mike Waddington, Evan Kane, Ronald Daanen, and Bill Cable. In addition, we would like to acknowledge the USGS Fairbanks Field Office, the USGS Office of Groundwater Branch of Geophysics (including Fred Day-Lewis and John Lane), the USGS Alaska Science Center, and support from USGS Pacific Coastal and Marine Science Center. The IAEA is grateful for the support provided to its Environment Laboratories by the Government of the Principality of Monaco. We thank Burke Minsley, Stephanie James, Tom Douglas, Vladimir Romanovsky, Jack McFarland, Kristen Manies, Ferdinand Oberle, and several anonymous reviewers for valuable comments on this work. Other field information relevant to this report can be found at "Field Activity Details for field activity 2014-624-FA" https://cmgds.marine.usgs.gov/fan_info.php?fan=2014-624-FA. The data used this study are openly available in Science Base https://doi.org/10.5066/P9KTHH8X. Any use of trade, product, or firm names in this publication is for descriptive purposes only and does not imply endorsement by the U.S. Government.

Queries for eego-25-02-04

This article has been typeset from the submitted materials. Check proofs carefully for conversion or other inadvertent errors. Please follow the Allen Press Guide to PDF Annotation when marking revisions. Do not edit the PDF directly.

If present, queries will be listed below with corresponding numbers in the margins or may appear as PDF comments addressed to the author or editor. If a correction is desired in response to a query, mark the necessary changes directly in the proof using the appropriate annotation tool. If no change is desired, no action is necessary in response.